Analysis of the Experimental Implications of the Scaling Theory of Polymer Adsorption

Jacob Klein*,† and Giuseppe Rossi*,‡

Weizmann Institute of Science, Rehovot 76100, Israel, and Mail Drop 3083/SRL, Ford Research Laboratory, Ford Motor Company, P.O. Box 2053, Dearborn, Michigan 48121-2053

Received June 24, 1997; Revised Manuscript Received January 6, 1998

ABSTRACT: A detailed analysis of the experimental implications of the scaling theory of polymer adsorption in the good solvent regime is presented. A number of new results that simplify the task of comparing theoretical predictions and experimental data are given: these include a new simple approximate expression for the force vs distance profile, which is close to the exact solutions over an appreciable range of the intersurface separations. The theoretical predictions are compared to available experimental data for the forces arising between mica plates exposed to poly(ethylene oxide)−water solutions. Good quantitative agreement between theory and experiment is found, with no need for adjustable parameters.

I. Introduction

Processes involving polymer layers adsorbed from solutions have considerable practical implications and at the same time continue to present a scientific challenge. This is because of their relevance to situations of technological importance such as lubrication and colloidal stabilization and, on the other hand, because these processes provide a rich testing ground for our theoretical understanding of confined polymer solvent systems.

Two significantly different approaches to predict the properties of these systems have evolved over the years. A set of theoretical and lattice computational methods, sometimes referred to as "numerical mean field theory" has been extensively used by Scheutjens, Fleer, and their collaborators.[1,2] In this formulation each polymer chain is represented by a step weighted walk. The equations for the statistical weights are solved numerically: it is then possible to obtain not just predictions for the polymer concentration profile but also more specific information on chain statistics, such as, for example, the probability that a chain segment located at a distance z from the adsorbing surface belongs to either a loop (a region of the chain located between two surface contact points) or a tail (a region of the chain located between a surface contact and an end point).

A different approach largely based on the analogy between the polymer adsorption problem and the theory of critical phenomena relies on the minimization of an appropriate surface free energy functional.[3,4] The form of the functional is chosen so as to reflect the main features of the physics for the situation that needs to be described. In particular, different forms of the surface free energy are used depending on solvent quality[3−6] (good vs Θ vs poor solvent) and on concentration level (dilute vs semidilute vs concentrated solutions). Until recently only functionals involving a single order parameter had been considered: at the mean field level this amounts to the so-called ground state dominance approximation.[7] As long as a single order parameter is used, predictions can be obtained for the polymer concentration profile and for the force between adsorbed layers.[3,4,8,9] However, to determine the relative contributions of loops, tails and free chains to the polymer concentration at a given distance from the adsorbing wall, it is necessary to introduce surface free energy functionals that involve more than one order parameter. Formulations of this type have been recently put forward[10,11] and the results have been compared to the corresponding numerical mean field theory results.[12]

In this paper we revisit the problem of interactions between surfaces carrying irreversibly adsorbed polymer chains across a good solvent medium. When the polymer is adsorbed to saturation, one expects a monotonic repulsion between the surfaces as they approach, resulting—for the case of colloidal particles—in the well-known steric stabilization of dispersions by adsorbed polymers. For undersaturated surfaces, attraction due to bridging may occur. Such attraction can have important practical consequences for destabilizing colloidal dispersions. Studies with surface force balances provide a very direct measure of the variation of the intersurface forces with surface separation and enable a critical comparison with molecular models. Here in particular we reexamine the surface force data collected in the good solvent regime for the poly(ethylene oxide), PEO/water, and for the PEO/toluene systems.[13−16] As shown in Figure 1 there is remarkable qualitative agreement between these results and the predictions of the (single order parameter) scaling theory. For unsaturated (starved) surfaces the theory predicts attractive interactions at long distances and repulsion when the surfaces are brought close to each other. The attractive minimum becomes shallower and its location is moved to larger distances as the amount of polymer adsorbed on the surfaces increases (see Figure 1a), until, at saturation, the theory predicts repulsion at all distances. The experimental results of refs 13−15 display the same qualitative behavior. As the incubation time of the mica plates in contact with the solution increases, the attractive minimum becomes less pronounced and is found at larger and larger interplate separations (see Figure 1b) until for sufficiently long incubation times (corresponding to adsorption to saturation) only repulsion is observed.

† Weizmann Institute of Science.
‡ Ford Motor Company.

S0024-9297(97)00931-5 CCC: $15.00
Published on Web 03/06/1998

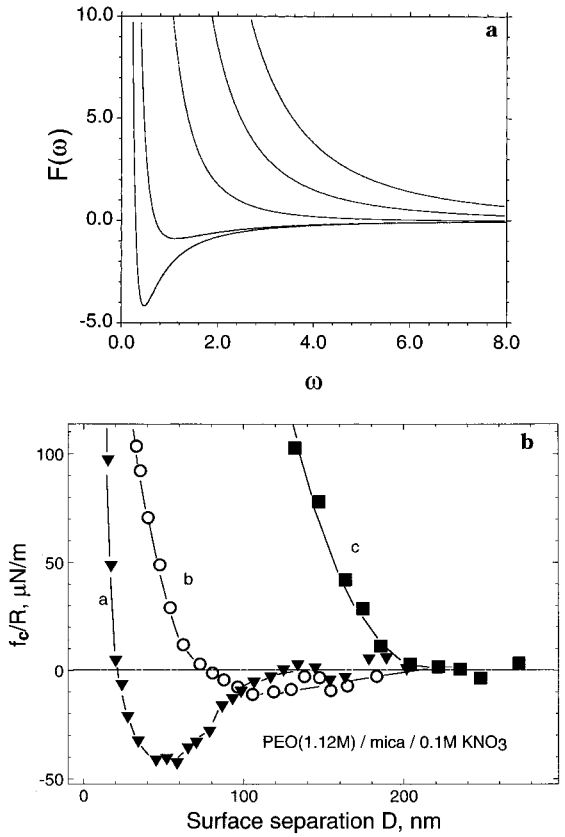

Figure 1. (a) Reduced force $F(\omega)$ vs interplate separation $\omega = 2h/D_{sc}$ predicted[8] from the single order parameter scaling theory for different values of saturation. From left to right the curves refer to $\Gamma/\Gamma_0 = 0.25$, 0.3, 0.5, 0.75, and 1.0. For $\Gamma/\Gamma_0 = 0.5$ and $\Gamma/\Gamma_0 = 0.75$, the attraction minimum falls outside the range of ω displayed in the figure. (b) Normalized experimental force vs distance profiles, f_c/R vs D, between two cylindrical mica surfaces (mean radius of curvature R) bearing adsorbed poly(ethylene oxide) across an aqueous medium 0.1 mol dm^{-3} KNO_3 at 23 ± 2 °C. The different sets of data correspond to increasing incubation times t_{inc} of the surfaces in the polymer solution and thus to increasing extent of adsorbance of polymer on the surfaces: a (triangles) $t_{inc} = 3$ h; b (circles), $t_{inc} = 8$ h; c (squares), $t_{inc} = 48$ h (saturated surface). Data were taken from ref 15.

In view of this kind of qualitative agreement, it is somewhat surprising that a systematic effort to interpret experimental data using the scaling description cannot be found in the literature. Indeed there has been a tendency to use instead the numerical mean field approach,[1] even though this neglects the excluded volume correlations that are known to play a crucial role in good solvents. The purpose of the present paper is two-fold: first we try to redress the situation described above, by performing a detailed comparison between the theoretical predictions of the scaling theory and the experimental data of refs 13−16. The second objective of this paper is to provide a set of tools that we believe will be of considerable use to experimentalists for the analysis of their results in terms of the scaling theory and for the design of new experiments, as well as a priori prediction of steric stabilization forces in colloidal dispersions.

A number of comments and caveats are in order at this point. First, it should be noted that the experimental protocol followed by Klein and Luckham differs somewhat from the situation to which the theoretical calculations of refs 8 and 9 refer. This is because the experiments do not involve any washing stage, that is a replacement of the solution with pure solvent prior to the force measurement. Despite this difference, it is still appropriate to compare the two sets of results, since the bulk concentration of free polymer in the experiments is very low. Indeed, during a force measurement involving starved plates, no free chains should be left between the plates when the interplate distance falls below $\sim R_g$, in the range where the theory does apply.[17]

A second caveat concerns the applicability of the scaling theory of ref 3 to the PEO−water system.[18] This system does involve dipole−dipole interactions, and it is not clear whether the long range nature of these forces causes any modification, other than a trivial rescaling of lengths, to the standard description of polymer solvent interaction in the good solvent regime. This description was developed under the assumption that only short range (van der Waals) interactions are present. In practice, for the salt concentrations used in the experiments,[19] it should be safe to ignore long-range dipole−dipole interactions.

Finally, it should be noted that a significant new prediction of the theory of polymer adsorption based on more than a single order parameter,[10−11] concerns the form of the force vs distance profile for surfaces carrying reversibly adsorbed polymer. The earlier single order parameter approach predicted that at full equilibrium the force would be attractive at any distance; by contrast, a repulsive long distance tail is found in the new formulation.[20−22] In the present paper we deal with irreversibly adsorbed chains rather than with reversible adsorption,[23] and we have chosen to compare our results with the predictions of the single order parameter formulation. We believe that it is more appropriate to compare experimental results for adsorbed polymers in good solvents with the predictions of the scaling model (despite its single order parameter approach), for the following reasons. First the treatments of the two plates problem within the two order parameter model, given thus far, still ignore excluded volume correlations and so do not make contact with the known solution behavior of polymers in semidilute solutions in good solvents.[24] Second, even for reversible adsorption, a direct estimate[22] using the results for the repulsive force reported in ref 20 shows that the predicted size of the repulsive interaction is within the experimental error limits associated to a surface force apparatus.

This paper is organized as follows. In the next section we summarize the scaling approach: we give a number of new numerical results for both the force between adsorbed layers and the surface free energy; we also derive two new simple approximate expressions for the force and for the surface free energy in the limit of small interplate separations. These results provide the necessary apparatus for the comparison between theory and experiments. In the third section, we apply these tools to the experimental results of Klein and Luckham. A brief summary and conclusions are given in the last section.

II. Predictions of the Scaling Theory of Polymer Adsorption

The scaling theory of polymer adsorption is based on the minimization of a surface free energy functional which is the sum of a surface term and a bulk contribution. The surface term accounts for the short-range attractive interactions between the surface and the monomers in immediate contact with it and depends

only on the value of the polymer volume fraction at the surface.[25] The bulk contribution is made up of an entropic and of an interaction (excluded volume) term: in this respect it resembles earlier mean field treatments of the problem.[26,27] However, the functional dependence of these two terms on the local polymer volume fraction is chosen so as to reproduce the scaling laws appropriate to the good solvent regime. These guidelines, coupled with simple dimensional considerations, led de Gennes[3,4] to propose for the surface free energy functional the form[28]

$$\gamma - \gamma_0 = -|\gamma_1|\Phi_s + \alpha kT \int_0^h dz \frac{1}{\xi^3(\Phi)}\left[1 + \left(m_0 \frac{\xi(\Phi)}{\Phi}\frac{d\Phi}{dz}\right)^2\right] \quad (1)$$

Here γ and γ_0 represent the surface free energy of the solution and of the pure solvent, respectively. $\Phi(z)$ is the value of the polymer volume fraction at a distance z from the adsorbing surface and $\Phi_s = \Phi(z = 0)$. γ_1 is a local solute−interface interaction energy per unit area (it is negative for adsorbing walls). $\xi(\Phi) = a\Phi^{-3/4}$ is the local correlation length, and a equals the effective monomer size. α and m_0 are numerical constants that can in principle be determined from experimental measurements in bulk solutions: notably α can be estimated from osmotic pressure data (see also section III) and m_0 from light scattering experiments.[4] The first term on the rhs of eq 1 is the short-range surface contribution[25] and the integral accounts for the bulk contribution: the first term in the integrand is the local interaction density associated with the polymer segments, while the squared gradient term represents the (mainly entropic) cost of maintaining the nonuniform segment composition profile within the adsorbed layer. The upper limit $z = h$ of the integration range corresponds to midgap for situations where two adsorbing plates are present; for a single plate $h = \infty$.

The surface free energy functional of eq 1 depends on four phenomenological (experimental) constants namely a, α, m_0, and γ_1. As we shall see, these constants can be directly related in the model to other experimentally measurable features, such as the shape of the segment density profile. Thus the quantitative predictions of the model for interactions between two surfaces can be obtained directly from measurements on an adsorbed layer at a single surface. Equation 1 can be developed to yield explicitly the composition profiles of the adsorbed layers, as well as the interaction between the two polymer-bearing surfaces as a function of the distance between them, and this has been done in detail in refs 3, 4, 8, and 9. Below we write down the main results derived in these earlier references which will be required for the experimental comparisons made later in this paper.

For irreversible adsorption the functional of eq 1 must be minimized subject to the constraint that the total amount of polymer, 2 Γ, in the interplate region is fixed. Here

$$\Gamma = \int_0^h \frac{\Phi(z)}{a^3} dz \quad (2)$$

In practice, in place of the constants m_0 and γ_1, it is convenient to introduce the length $m = 8am_0/3$ and the scaling length D_{sc}. The latter is defined by writing the boundary condition at the adsorbing surface (obtained[9] by minimizing $\gamma - \gamma_0$ with respect to Φ_s) as

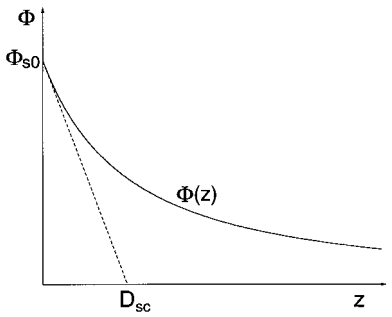

Figure 2. Values of Φ_{s0} and D_{sc} obtained from a single (saturated) surface segment depth profile $\Phi(z)$ as indicated: here D_{sc} is the intercept of the tangent to $\Phi(z)$ at the surface. Experimentally, such profiles are measured using neutron scattering or reflectometry.[41,42]

$$-\frac{1}{\Phi_s}\frac{d\Phi}{dz}\Big|_s = \frac{1}{D_{sc}}\left(\frac{\Phi_s}{\Phi_{s0}}\right)^{1/4} \quad (3)$$

where Φ_{s0}, the surface concentration of a single saturated plate, can be shown[9] to be related to m and D_{sc} by

$$\Phi_{s0} = \left(\frac{3m}{8D_{sc}}\right)^{4/3} \quad (4)$$

and to the coverage for a single saturated plate, Γ_0, by

$$a^3\Gamma_0 = 4D_{sc}\Phi_{s0} \quad (5)$$

From eq 3 we see that both Φ_{s0} and D_{sc} may be obtained directly from the single surface segment concentration profile for the saturated case, as indicated in Figure 2. Furthermore it can be shown[4,8,9] that

$$D_{sc} = \frac{9\alpha kTm^2}{32|\gamma_1|a^3\Phi_{s0}^{1/4}} \quad (6)$$

The result of the minimization procedure[8,9] are two closed integral relations connecting the surface, Φ_s, and the midpoint, $\Phi_m = \Phi(z = h)$, concentrations to h/D_{sc} and Γ/Γ_0. These relations are

$$\frac{h}{4D_{sc}} = \int_{y_m}^{y_s} dy \left(\frac{y}{y^9 - y_m^9 - \tilde{\mu}(y^4 - y_m^4)}\right)^{1/2} \quad (7a)$$

$$\frac{\Gamma}{\Gamma_0} = \int_{y_m}^{y_s} dy \left(\frac{y^9}{y^9 - y_m^9 - \tilde{\mu}(y^4 - y_m^4)}\right)^{1/2} \quad (7b)$$

Here $y^4(z) = \Phi(z)/\Phi_{s0}$, $y_s = y(z = 0)$, $y_m = y(z = h)$ and

$$\tilde{\mu} = \frac{(y_s^9 - y_m^9 - y_s^5)}{(y_s^4 - y_m^4)} \quad (8)$$

From the values of y_m and y_s corresponding to given $h/4D_{sc}$ and Γ/Γ_0, it is possible to obtain the concentration profile, by inverting (solving for $y(z)$) the integral relation

$$\frac{z}{4D_{sc}} = \int_{y(z)}^{y_s} dy \left(\frac{y}{y^9 - y_m^9 - \tilde{\mu}(y^4 - y_m^4)}\right)^{1/2} \quad (9)$$

To get the interplate pressure Π_d as a function of interplate separation only y_m is needed, since it can be shown[4] that

$$\Pi_d = -\frac{\partial(2\gamma)}{\partial(2h)} = -\frac{\partial\gamma}{\partial h} = \frac{\alpha kT}{a^3}(\tilde{\mu}\Phi_m\Phi_{s0}^{5/4} - \Phi_m^{9/4}) \quad (10)$$

If the quantities in the rhs of eq 10 are evaluated at $z = h$, then Π_d is the interplate pressure between two plates located a distance $2h$ apart. In practice, it has become customary to report the reduced function[29] $F(\omega)$, where $\omega = 2h/D_{sc}$. This is related to $\Pi_d(h)$ by[30]

$$\Pi_d(2h) = \frac{\alpha kT}{a^3}\Phi_{s0}^{9/4}F(\omega) \quad (11)$$

In measurements performed with the surface force apparatus,[31,32] what is measured is the force f_c acting between the (adsorbed) surfaces of a pair of crossed cylinders, rather than between two plates. It can be shown[33] that, if R is the cylinders' radius and D the minimum distance between the cylinders, $f_c(D)$ is to a good approximation given by

$$\frac{f_c(D)}{R} \approx 4\pi\tilde{\gamma}(h = D/2) = 4\pi\int_D^\infty \Pi_d(z)\,dz \quad (12)$$

Here we introduced the quantity $\tilde{\gamma}(h = D/2)$ defined by the integral on the rhs of eq 12. By virtue of eq 10, $\tilde{\gamma}$ coincides with the surface free energy γ of eq 1 up to an integration constant.[34] In analogy to (11) we can introduce a reduced surface energy function $G(\omega)$ related to $\tilde{\gamma}$ by

$$\tilde{\gamma}(h) = \frac{\alpha kT}{a^3}\Phi_{s0}^{9/4}\frac{D_{sc}}{2}\int_\omega^\infty F(\omega)\,d\omega = \frac{\alpha kT}{a^3}\Phi_{s0}^{9/4}\frac{D_{sc}}{2}G(\omega) \quad (13)$$

While eqs 7−9 provide a closed form solution of the minimization problem, it is clear that, in general, numerical methods have to be used in order to invert these relations, to obtain y_m, y_s, and $y(z)$ for a given ω and Γ/Γ_0. Examples of numerical results of this kind were given in refs 8 and 9. However, the emphasis in those papers was on the qualitative form of the results, rather than on providing a tool to compare the predictions of the theory with experimental data. As a result, $G(\omega)$ was not computed in those papers, and the linear−linear plots of the interplate pressure vs distance profile that were given there are useful in determining the depth and location of the minima of $F(\omega)$ only for a restricted range (around $\Gamma/\Gamma_0 \approx 0.3$) of coverage values. As we shall see in detail in the next section, this range does not correspond to the range of undersaturations investigated experimentally by Klein and Luckham. To remedy this situation we give in Figures 3−5 a number of "master" curves. From these curves it is possible to determine directly the salient features of both the interplate pressure vs distance and the surface energy vs distance profiles for the entire range of coverages that is likely to be of interest experimentally. Detailed examples of how these master curves are used to compare with experimental data are presented in section III.

Parts a and b of Figure 3, display, respectively on a linear−linear and a log−log scale, the shape of the

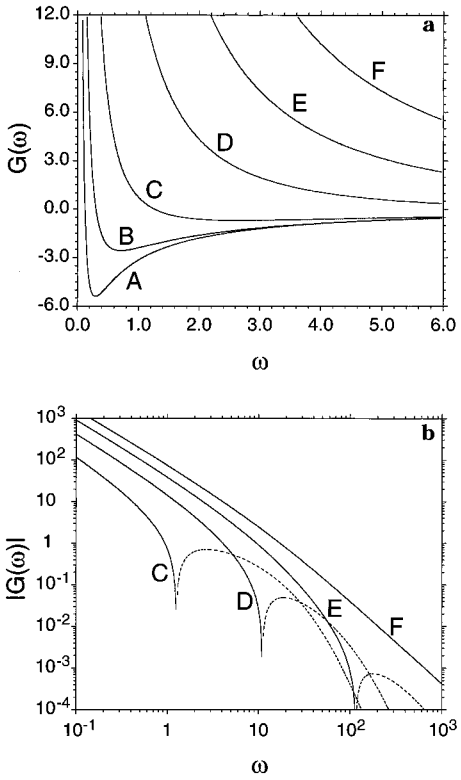

Figure 3. (a) Reduced surface free energy $G(\omega)$ vs interplate separation $\omega = 2h/D_{sc}$ predicted from the single order parameter scaling theory for different values of saturation: the curves refer to $\Gamma/\Gamma_0 = 0.25$ (curve A), 0.3 (curve B), 0.4 (curve C), 0.6 (curve D), 0.8 (curve E), and 1.0 (curve F). (b) The absolute value of the reduced surface free energy of part a shown on a log−log scale: the curves refer to $\Gamma/\Gamma_0 = 0.4$ (curve C), 0.6 (curve D), 0.8 (curve E), and 1.0 (curve F). Each curve (except F) has two branches corresponding to the repulsive (continuous curves) and attractive (broken curves) portion of the data of Figure 3a.

reduced surface energy function $G(\omega)$ for a number of different coverage levels. As noted in the discussion preceding eq 12, $G(\omega)$, rather than $F(\omega)$, is the quantity of interest in comparisons between theory and force measurement involving curved surfaces (the measurements of refs 13−15). The log−log plots of Figure 3b are provided in order to allow a quantitative estimate of $G(\omega)$ even for values of Γ/Γ_0 that are too large to exhibit attraction within the range of ω covered by Figure 3a. For any $\Gamma/\Gamma_0 < 1$, i.e., for undersaturated surfaces, one expects a bridging attraction followed by an osmotic repulsion on closer approach, so that $G(\omega)$ changes sign at some finite value ω_0 of ω: it is positive (repulsion) for $\omega < \omega_0$ and negative (attraction) for $\omega > \omega_0$. As a result, in Figure 3b each dataset corresponding to a given ratio $\Gamma/\Gamma_0 < 1$ (C, D, and E) has two branches, one for the repulsive (continuous curves) and the other for the attractive (broken curves) portion of the corresponding curves in Figure 3a.

The locations and the depths of the minima of both $F(\omega)$ and $G(\omega)$ as functions of Γ/Γ_0 are displayed in linear−log form in Figures 4 and 5, respectively. Figure 4 also gives (curve C) the location of the zero of $G(\omega)$. The insets in these figures indicate which quantities each curve represents. For example, in Figure 4, curve A gives the location of the minimum of $F(\omega)$ and curve B gives the location of the minimum of $G(\omega)$. Since G is obtained from F by a simple quadrature, the minimum of $G(\omega)$ is found at the value of ω where F changes

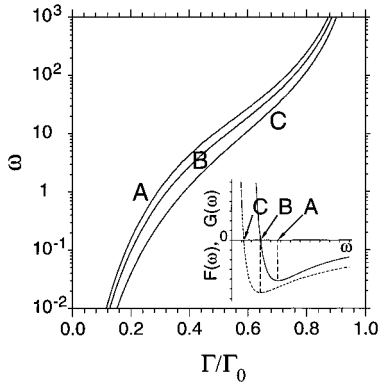

Figure 4. Location ω of the minima of the reduced force $F(\omega)$ (curve A), of the reduced surface free energy $G(\omega)$ (curve B) and of the zero of $G(\omega)$ (curve C) as a function of coverage Γ/Γ_0. The quantities plotted in each of these three curves are shown in the inset (lower right corner): the two curves in the inset are computed numerical results for $F(w)$ (continuous curve) and $G(w)$ (broken curve) for a given value of the ratio Γ/Γ_0.

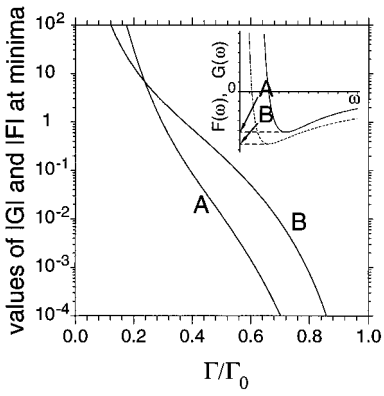

Figure 5. Depths of the attractive minima of $F(\omega)$ (curve A) and of $G(\omega)$ (curve B) as a function of coverage Γ/Γ_0. The inset in the upper right corner shows the quantity plotted in each curve. The two curves in the inset are computed numerical results for $F(w)$ (continuous curve) and $G(w)$ (broken curve) for a given value of the ratio Γ/Γ_0.

sign. In Figure 5, curve A gives the depth of the minimum of $F(\omega)$ and curve B the depth of the minimum of $G(\omega)$. The curves of Figure 5 do intersect at small Γ/Γ_0; this is because at low Γ/Γ_0 the range of ω where F is significantly smaller than zero is very narrow so that the integrated negative contribution to $G(\omega)$ (see eq 13) is small.

There is an additional point of interest concerning comparison of the theoretical predictions of the scaling model with experiment. For the case of fully saturated surfaces, in the limit of large gaps (though where the layers are still in overlap, sometimes called the central regime[4]), we expect the surface pressure to vary as $\Pi_d \propto kT/h^3$, as pointed out long ago.[4,35] We may examine the range of interactions over which this central-regime limit holds. From eqs 4 and 11, we have $\Pi_d \propto F(\omega)/D_{sc}{}^3$, so that $F(\omega) \sim (h/D_{sc})^{-3} \sim \omega^{-3}$ in the central regime limit. That is, in this limit $\omega^3 F(\omega)$ should be a constant, and the magnitude of Π_d should be independent of the value of D_{sc}. The quantity $\omega^3 F(\omega)$ for saturated surfaces is plotted in Figure 6 on a log−log scale; it is seen that it indeed becomes constant, as expected at large ω, but it is of interest that even over a 2 orders of magnitude variation $\omega = 10-1000$ (which includes experimentally relevant values of the gap, see next section), $\omega^3 F(\omega)$ varies only by a factor of 2. If we take the limiting

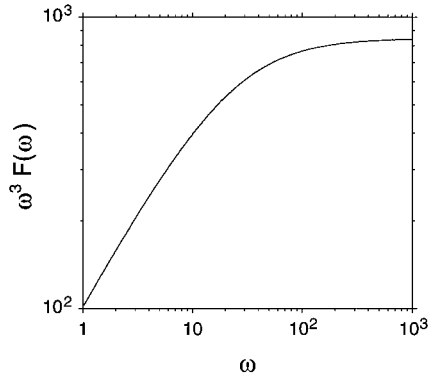

Figure 6. Plots of the quantity $\omega^3 F(\omega)$ vs $\omega = 2h/D_{sc}$ for saturated surfaces, $\Gamma/\Gamma_0 = 1.0$. This figure illustrates the independence of the interplate pressure Π_d of D_{sc} at large ω.

(constant) value of $\omega^3 F(\omega)$ as C_0, e.g., $C_0 \cong 8.5 \times 10^2$ (see Figure 6), then from eqs 4 and 11 we have, for the central regime or large gap limit

$$\Pi_d = \frac{\alpha kT(3m)^3}{a^3}\frac{C_0}{h^3} \tag{14}$$

independent of D_{sc} and of Φ_{s0}.

While the "master" curves provided in Figures 3−5 should greatly facilitate comparison between theory and experiments, it is often of value to have closed form expressions to describe and fit the data. In this context, we have made a remarkable finding: if the gradient square term in eq 1 is neglected, it is easy to obtain simple analytical expressions for both $F(\omega)$ and $G(\omega)$ that approximate surprisingly well the actual form of these functions. This is true even at relatively large values of ω, although strictly speaking the approximations are exact only in the limit $\omega \to 0$. To derive these expressions we start from the situation where the interplate separation is so small that the concentration profile $\Phi(z)$ between the plates is essentially flat. Then the values of the concentration at the surface Φ_s and at the midpoint Φ_m nearly coincide and one has $\Phi(z) \approx \Phi_s \approx \Phi_m \approx (\Gamma a^3)/h$. As a result, the square gradient term in the integrand on the rhs of eq 1 can be neglected. Under this assumption, the integral in eq 1 is readily evaluated, giving

$$\gamma - \gamma_0 \approx -|\gamma_1|\Phi_s + \frac{\alpha kT}{a^3}h\Phi_m{}^{9/4} \approx -\frac{|\gamma_1|\Gamma a^3}{h} + \frac{\alpha kT}{a^3}\frac{(\Gamma a^3)^{9/4}}{h^{5/4}} \tag{15}$$

Thus using (4), (5), and (6), one finds

$$\gamma - \gamma_0 \approx \frac{\alpha kT}{a^3}\Phi_{s0}{}^{9/4}\frac{D_{sc}}{2}\left[-\frac{32\Gamma}{w\Gamma_0} + \frac{1}{w^{5/4}}\left(\frac{8\Gamma}{\Gamma_0}\right)^{9/4}\right] \tag{16}$$

so that

$$\Pi_d = -\frac{\partial\gamma}{\partial h} = -\frac{2}{D_{sc}}\frac{\partial\gamma}{\partial w} \approx \frac{\alpha kT}{a^3}\Phi_{s0}{}^{9/4}\left[-\frac{32\Gamma}{w^2\Gamma_0} + \frac{5}{4}\left(\frac{8\Gamma}{w\Gamma_0}\right)^{9/4}\right] \tag{17}$$

The two expressions in square brackets in the rhs of eqs 16 and 17 give $G(w)$ and $F(w)$ respectively[34] in the

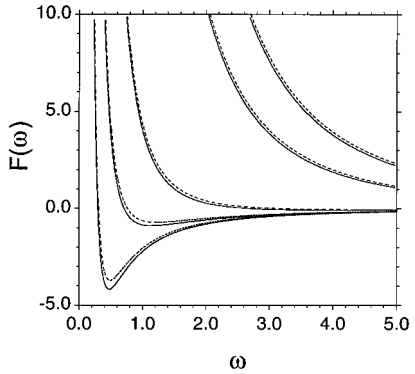

Figure 7. Comparison of (small ω) estimates of $F(\omega)$ obtained from eq 19 (broken curves) with actual values of $F(\omega)$ obtained from the full minimization procedure (continuous curves), for (from left to right) $\Gamma/\Gamma_0 = 0.25$, 0.3, 0.4, 0.8, and 1.0.

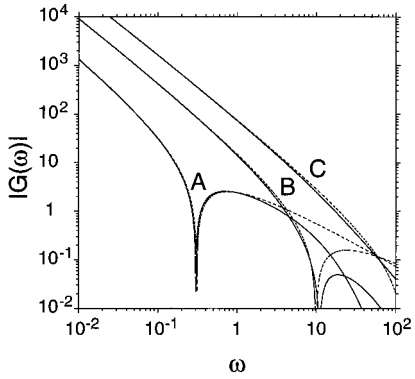

Figure 8. Comparison of estimates for $G(\omega)$ obtained from eq 18 (broken curves) with actual values of $G(\omega)$ obtained from the full minimization procedure (continuous curves). The results shown here refer to $\Gamma/\Gamma_0 = 0.3$ (curve A), 0.6 (curve B), and 1.0 (curve C).

limit $w = 2h/D_{sc} \rightarrow 0$. In other words

$$G(\omega) \approx -\frac{32\Gamma}{w\Gamma_0} + \frac{1}{w^{5/4}}\left(\frac{8\Gamma}{\Gamma_0}\right)^{9/4} \tag{18}$$

$$F(\omega) \approx -\frac{32\Gamma}{w^2\Gamma_0} + \frac{5}{4}\left(\frac{8\Gamma}{w\Gamma_0}\right)^{9/4} \tag{19}$$

Figure 7 shows how results for $F(\omega)$ obtained from eq 19 for different values of Γ/Γ_0 (broken curves) compare to the corresponding results found numerically from eqs 7 and 10 (continuous curves). It is evident from this figure that eq 19 reproduces quite well both the position of the attractive minima and the shape of the curves in the whole range of ω shown in the figure. In fact, the approximate expressions (18) and (19) appear to work well for the repulsive portion of both $F(\omega)$ and $G(\omega)$ at even larger values of ω. This can be seen from the log−log plots of Figure 8, which show how the approximation for $G(\omega)$ (broken curves) obtained from eq 18 compares with the corresponding results found numerically from eqs 7, 10, and 13 (continuous curves). Note, however, that the approximate expressions are not as good in describing the behavior of G in the attractive region at large ω. Thus, while the spatial aspects of the approximate expressions—for example the positions of the minimum in $G(\omega)$ and of the crossover from attraction to repulsion—are close to the exact results, the magnitude of G in the attractive region is less satisfactory when compared to the full numerical calculations.

These results point to the fact that the physics of the system is largely dominated by the interplay between the short distance attraction represented by the first term in eqs 18 and 19 and the excluded volume repulsion accounted for by the second term. It is only at relatively large separation that the entropic interactions, represented by the gradient square term in the integrand on the rhs of eq 1, begin to contribute significantly to the interplate pressure. This is the reason the approximate expressions give a relatively poorer description of the attractive tail region in the undersaturated case, which is dominant at the larger surface separations.

III. Comparison of Experiments with Predictions of the Scaling Model

In this section we compare the predictions of the scaling model described above with measurements of the forces between polymer-bearing surfaces in good solvents using the surface force balance (SFB). These provide the most direct and unambiguous comparison between theory and experiment and enable a critical evaluation of the applicability of the model. We start by examining the more common case of interactions between surfaces onto which polymer has adsorbed to saturation.[14,16] Later in this section we compare with interactions between undersaturated surfaces,[13,15] where bridging attractions can dominate over a sizable regime of the surface separation (see also Figure 1). We shall use the results from the SFB studies for interactions between mica surfaces bearing adsorbed poly(ethylene oxide) (PEO) across aqueous solutions[13−15] and across toluene,[16] which are moderately good to good solvents for the polymer.

(a) Interactions for Saturated Coverage. We note first an important qualitative feature of the scaling model for saturated surfaces (full coverage) that has to do with the range and magnitude of the interactions. Within the model, interactions are calculated for the case when the layers are already in some overlap (and where the concentrations are in the semidilute regime). In this regime (sometimes called the central, or weak overlap regime) the predictions of the model for the surface pressure Π_d or the interaction energies $\tilde{\gamma}$ (see eqs 11−13) are independent of the polymer molecular weight M. In practice, we expect that the onset of interactions between adsorbed layers takes place when they first come into contact, at surface separations $D = D_{onset}$ of the order of a few R_F, the swollen Flory dimension ($R_F \propto M^{3/5}$). This is the size of the largest loops or tails of the adsorbed layers extending from the surface. Thus D_{onset} is expected to be a function of the molecular weight M of the adsorbed chains. The picture then is one where we expect the predictions of the model to be independent of M within a surface separation regime, defined by the overlap of the adsorbed layers, which does depend on M.

This picture may be examined using the results of the SFB studies, as shown in Figures 9 and 10. Figure 9 shows the normalized force−distance profile $f_c(D)/R$ between crossed cylindrical mica surfaces (here R is the mean radius of curvature of the surfaces) bearing a saturated surface layer of PEO in aqueous 0.1 M KNO_3.[14] Here D is the separation of closest approach between the surfaces. The normalized plot is equivalent (within a prefactor 4π; see eq 12) to the surface energy $\tilde{\gamma}$ for interacting plane parallel plates a distance $D = 2h$ apart. Two molecular weights are shown, $M =$

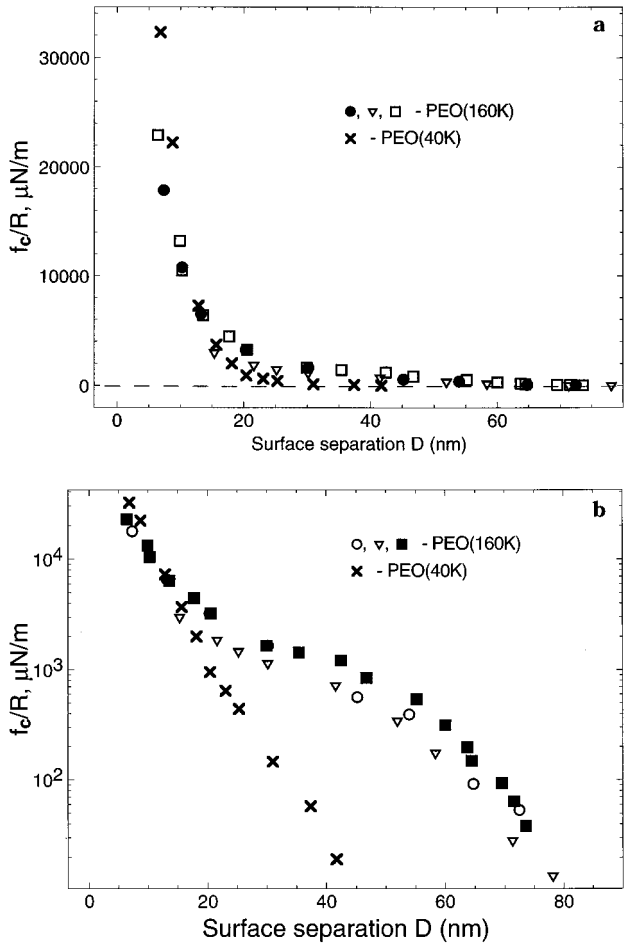

Figure 9. (a) Normalized experimental force vs distance profiles f_c/R vs D between curved mica surfaces (mean radius of curvature R) bearing adsorbed poly(ethylene oxide) across an aqueous medium (0.1 M KNO_3), following adsorption to saturation. Different symbols labeled PEO(M) correspond to different molecular weights M of the polymers. (b) As in part a but on a semilogarithmic plot, showing clearly both the different onset separations at which repulsive forces are seen for the different M values, and the region ($D \approx 25$ nm) over which the profiles merge. Data were taken from ref 14.

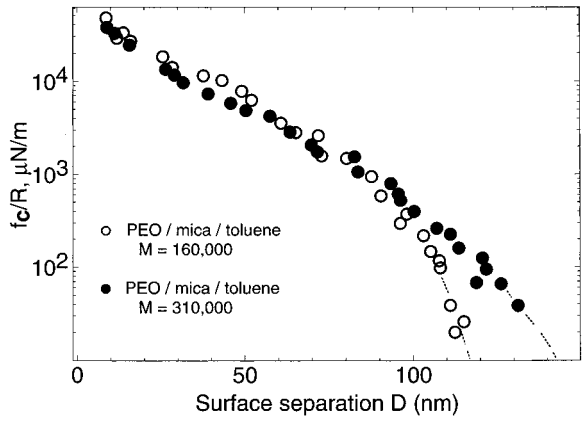

Figure 10. Normalized experimental force vs distance profiles f_c/R vs D between curved mica surfaces (mean radius of curvature R) bearing adsorbed poly(ethylene oxide) across toluene, following adsorption to saturation, on a semilogarithmic plot. Different symbols correspond to different molecular weights M of the polymers. Data were taken from ref 16.

40 000 and $M = 160\,000$. In the linear−linear representation of Figure 9a the two force profiles appear rather similar. Figure 9b shows the same data on a semilogarithmic plot: here the onset distance, of order a few R_F for each polymer (see later), is seen to be markedly larger for the longer molecules, as expected; the onset distance for the saturated curve of the 1.2 M PEO (Figure 1b, curve c) is even larger in line with the higher molecular weight of this polymer.[36] We particularly note, in line with the picture described above, that over the surface separation regime $D \lesssim 25$ nm the two profiles merge, becoming independent of M. In Figure 10 the force profiles between mica surfaces bearing adsorbed PEO across the good solvent toluene are shown,[16] again for two molecular weights ($M = 160\,000$ and $M = 310\,000$). The main qualitative features are clear: interactions commencing at distances of order of a few R_F for the respective polymers[37] (with onset for the longer chains starting sensibly further out) and then, for $D \lesssim 90$ nm for the data of Figure 10, the two force profiles merge, with the interaction profiles independent of M as predicted. The actual onset distances, for all polymers shown in Figures 9 and 10, are in the range $D_{onset} \cong (4-5)R_F$, suggesting an effective adsorbed layer thickness of some $(2-2.5)R_F$.[38,39]

While Figures 9 and 10 confirm the qualitative picture of the scaling model for interactions between adsorbed polymers, a quantitative comparison requires the full calculated form of Π_d or of $\tilde{\gamma}$ given by eq 11 or eq 13. For comparison with the SFB experiments, which yield f_c/R, we have, from eqs 12 and 13

$$\frac{f_c}{R} = 2\pi\left(\frac{\alpha kT}{a^3}\right)\Phi_{s0}^{9/4} D_{sc} G(\omega) \tag{20}$$

To obtain the value of $(\alpha kT/a^3)$ we recall the definition of the parameter α in terms of the osmotic pressure Π_{osm} of a semidilute polymer solution at volume fraction Φ

$$\left(\frac{\alpha kT}{a^3}\right) = \frac{4}{5}\Pi_{osm}\Phi^{-9/4} \tag{21}$$

At moderately high compressions, where the concentration profile across the intersurface gap is essentially flat, the osmotic pressure across the gap is constant and equals the intersurface pressure Π_d. In this limit the osmotic pressure may be evaluated from the relation

$$\Pi_{osm} \equiv \Pi_d = -\frac{1}{2\pi}\frac{\partial}{\partial D}\left(\frac{f_c}{R}\right) \tag{22}$$

and obtained from the experimentally determined f_c/R profiles. The mean volume fraction $\Phi(D)$ in the gap for the high compression region is given by $\Phi(D) = 2\,\Gamma/D$ (Γ being the adsorbance on each surface in units of length corresponding to the thickness of the equivalent polymer melt film).

To evaluate $(\alpha kT/a^3)$ for the case of the PEO/mica/0.1 M KNO_3 system we may use data from the SFB study of ref 14, for which force profiles are reproduced in Figure 9. For that system, $\Gamma = 4 \pm 1.5$ nm (for PEO of both molecular weights studied). From Figure 5 of that study,[14] we find for $D = 20$ nm, e.g., that $\partial(f_c/R)\partial D \cong -3 \times 10^5$ N/m^2. From eq 22 we evaluate Π_{osm} and from eq 21—using the appropriate value of $\Phi(D) = 2\,\Gamma/D$—we find $(\alpha kT/a^3) \cong 3 \times 10^5$ N/m^2 (similar values are obtained by considering the slope $\partial(f_c/R)/\partial D$ also at different values of D).

To calculate explicitly the predicted force profile from eq 20, we require values of the polymer volume fraction

Φ_{s0} at the single incubated surface and the value of the extrapolation length D_{sc}. These are most directly obtained from experimentally measured concentration vs depth profiles of the adsorbed polymers on the surface, as explained in Figure 2. We may use the data of Cosgrove and co-workers[41] and Lee et al.[42] who determined such profiles for PEO in aqueous solution adsorbed on polystyrene latices and on quartz. These profiles yield $\Phi_{s0} = 0.25-0.3$ and $D_{sc} = 4 \pm 1$ nm.[43] These values have some uncertainty due to experimental scatter and, in addition, are for adsorbing surfaces different from mica.[44] Bearing these reservations in mind, knowledge of Φ_{s0} and D_{sc} enables us, together with the experimentally determined value of $(\alpha kT/a^3)$, to make an explicit quantitative prediction of the force vs distance profile, eq 20, with no adjustable parameters. That is, all parameters in the theoretical expression for the force between two surfaces are determined directly from measurements on a single surface or on bulk polymer solution. For the particular values of Φ_{s0}, D_{sc}, and $(\alpha kT/a^3)$ for the system under consideration, the predicted surface force profile between adsorbed PEO layers in water becomes

$$\frac{f_c}{R} = 2\pi\left(\frac{\alpha kT}{a^3}\right)\Phi_{s0}^{9/4} D_{sc} G(\omega) = (330-500)G(\omega)\frac{\mu N}{m} \quad (23)$$

The uncertainty quoted here reflects only uncertainty in the value of Φ_{s0}; i.e., to obtain the prefactor in eq 23 we took $D_{sc} = 4$ nm and $\Phi_{s0} = 0.25-3$: note that scatter in D_{sc} leads to smaller variation in the prefactor than a comparable scatter in Φ_{s0}. The value of $G(\omega)$ for saturated surfaces is calculated as described above (eq 13 and following), and is given in the master curve F of Figure 3a,b.

In Figure 11 we compare the theoretical expression, eq 23 (solid curves), with data from the SFB experiments for the PEO/mica/0.1 M KNO_3 system.[14] The predicted profile, with no adjustable parameters, closely matches the data once overlap of the layers has occurred. This is clearly seen in the semilogarithmic plot in Figure 11b. We note also the good agreement with the data of the approximate analytic expression (broken curves in Figure 11) given by eq 18.

(b) Interactions for Undersaturated Coverage. As noted in section II, and shown in Figure 1b, interactions between undersaturated surfaces exhibit a net attraction over an appreciable regime of surface separations due to bridging by the adsorbed chains.[13,15] The interactions between curved surfaces in this case are still given by eq 20 (or eq 23 for the specific system considered); the difference from the saturated case is that the degree of undersaturation Γ/Γ_0 needs to be specified. We compare our calculations with the experimental force−distance curves a and b of Figure 1b (for the same system for which comparison was made above in the saturated case), which show clear bridging attraction.

In general there are different experimental methods for assessing the extent of saturation of a surface. These include force−distance profiles at high compression,[14] refractive index profiles[45] in the SFB, or more standard methods such as depletion of a polymer solution by an adsorbing colloidal dispersion or optical methods.[1] For curves a and b of Figure 1 we do not have independent measures of the undersaturation Γ/Γ_0, but we may estimate it as follows. The surface separation D_{min} at the minimum in the force profile f_c/R gives a measure of the value of $\omega = \omega_{min}$ at the minimum ($\omega_{min} = D_{min}/D_{sc}$). Using this value of ω_{min} and curve B of Figure 4, we read off the value of Γ/Γ_0; this gives a measure of the undersaturation for the experimental curve. We then calculate the corresponding $G(\omega)$ and, using eq 20 (or eq 23 in our case) we predict the full f_c/R profile. We expect that if the model is correct the predicted force profile, based on our estimate of the undersaturation, should self-consistently match the data not only with respect to the position of the minimum, but also as regards the magnitude and shape of the bridging attraction.

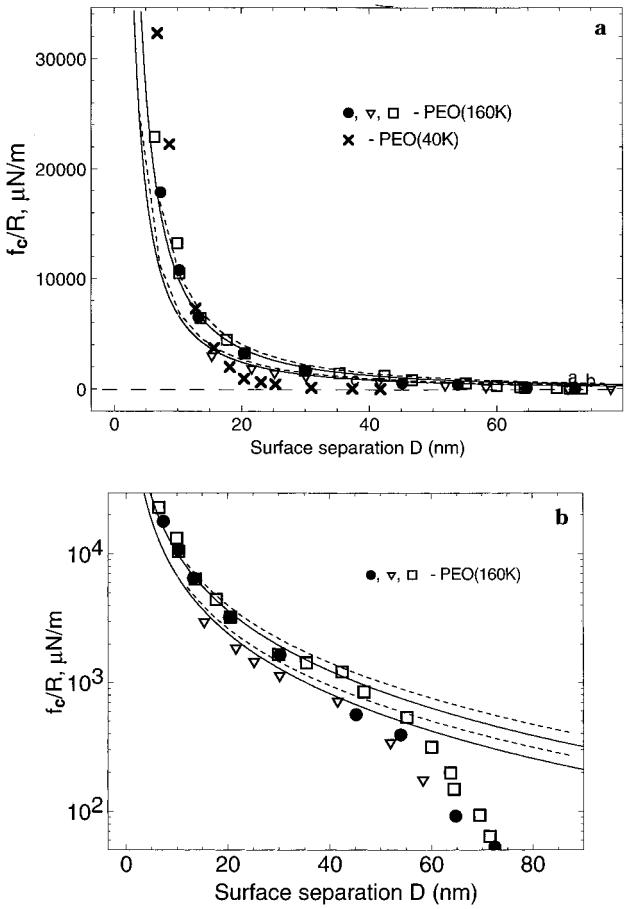

Figure 11. Comparison of calculated interaction profiles f_c/R (solid curves) for saturated polymer-bearing surfaces based on eq 20, with experimental profiles for the system described in Figure 9 (data from ref 14). The two solid curves span the range of predicted profiles (eq 23) corresponding to $(\alpha kT/a^3) = 3 \times 10^5$ N/m^2, $D_{sc} = 4$ nm, and $\Phi s0 = 0.25-0.3$ nm, with $G(\omega)$ calculated exactly. Broken curves are based on the approximate expression for $G(\omega)$ in eq 18. Key: (a) linear plot including both PEO molecular weights (see symbols); (b) Semilogarithmic plot of the data for PEO(160K).

The comparisons are shown in parts a and b of Figure 12. The data are taken from the force−distance profiles for undersaturated surfaces for the PEO/mica/0.1 M KNO_3 system[14] (Figure 1b, curves a and b, respectively); the corresponding predicted curves, based on eq 23, are shown in these figures as solid lines, where the undersaturation values estimated as above are $\Gamma/\Gamma_0 = 0.55 \pm 0.01$ and $\Gamma/\Gamma_0 = 0.64 \pm 0.01$, respectively. The agreement between theory and experiment, using exactly the same independently determined values of D_{sc} and Φ_{s0} as in Figure 11 for the saturated adsorption case, is close. We especially note that while the minima in the

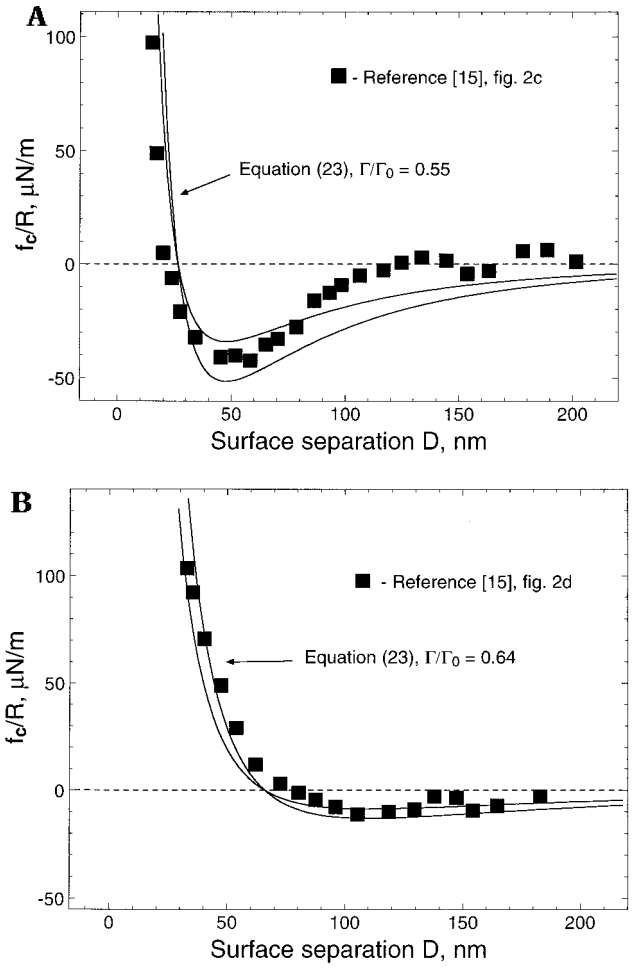

Figure 12. Comparison of calculated interaction profiles f_c/R (solid curves) for undersaturated polymer-bearing surfaces based on eq 23, with experimental profiles for the system described in Figure 1b (data from ref 15). The two solid curves span the range of predicted profiles (eq 23 with $G(\omega)$ calculated exactly) with parameters ($\alpha kT/a^3$), D_{sc}, and Φ_{s0} identical to those used in Figure 11 for undersaturation values Γ/Γ_0 estimated as described in text. Key: (a) Comparison with curve a of Figure 1b, $\Gamma/\Gamma_0 = 0.55$ (based on ref 15, Figure 2c); (b) Comparison with curve b of Figure 1b, $\Gamma/\Gamma_0 = 0.64$ (based on ref 15, Figure 2d).

predicted curves were chosen via Figure 4 to fit the experimental curves, to extract Γ/Γ_0, the absolute magnitude of the theoretical profiles, as well as their shape, is in very good agreement with the data, again with no adjustable parameters. There is some deviation at the largest separations, where the magnitude of the predicted attraction is larger than the experimentally measured values. The reason for the discrepancy is similar to that noted earlier for the case of repulsive interactions between saturated surfaces (Figure 11). It arises because the attractive interactions observed experimentally commence only when bridging by the adsorbed chains becomes possible, at $D \lesssim (2-3)R_F$ for the polymer shown in Figure 12, while the predicted curves are M independent. (We recall that for saturated surfaces repulsive interactions are observed only for $D < D_{onset} \approx (4-5)R_F$.)

IV. Summary and Conclusions

In this paper we present for the first time a comprehensive analysis of the implications of the scaling theory of adsorption for the experimental measurements of forces between polymer-bearing surfaces across good solvents, both for saturated and for undersaturated ("starved") surfaces. We present a number of master curves which can be used to predict the pressure–distance profile between flat parallel (polymer-bearing) plates, and the force–distance profile between curved surfaces. All parameters entering the predicted profiles for the two-surface interactions can be determined from measurements (such as osmotic pressure or light scattering) on bulk polymer solutions or from measurements (such as of polymer adsorbance or the segment density profile) on a single adsorbing surface. The regime of validity of the theory is for surface separations such that there is some overlap of the layers. In practice, and for the systems examined here, this is at separations less than some $(4 \pm 1)R_F$ for the polymers studied (covering a 30-fold molecular weight range (4×10^4 to 1.2×10^6)). We have also presented an approximate closed form for the interaction profiles, derived by ignoring the effect on the interaction energy of the concentration gradient. This closed form should be correct, strictly, at high compressions. It turns out, however, to do better than that and to approximate the exact solutions closely over a wide range of surface separations, thereby providing a useful analytical expression for surface interactions.

We performed a detailed comparison of our calculated results with previously published experimental force–distance profiles between surfaces bearing adsorbed polymer (PEO) in a marginally good solvent (aqueous 0.1 mol dm^{-3} KNO_3 at 23 ± 2 °C). Such profiles, measured with a surface force balance, provide the most direct testing ground for the theoretical predictions. We were able to estimate quantitatively all parameters entering the calculations directly from bulk and single-surface experimental measurements, and thus to predict the full two-surface interaction profiles with no adjustable parameters. The predicted profiles compare very well in magnitude and spatial scales with the experimental ones, both for fully saturated and for undersaturated surfaces.

Detailed comparisons have been made earlier of the predictions of mean field and self-consistent mean field models of polymer adsorption with surface force measurements in Θ[1,6] and poor[5,6] solvents. However, to our knowledge, this is the first detailed quantitative theory–experiment comparison of surface forces for the most common case of adsorption from a good solvent. The good agreement—in the absence of any adjustable parameters—suggests that the scaling model of polymer adsorption in good solvents, even in the relatively simple form originally written down by de Gennes,[4] is capable of providing a good quantitative description of such forces. The underlying reason for this is that despite its relatively simple form, eq 1 provides a description which takes into account properly the essential effect of excluded volume statistics; at the same time it enables the self-consistent evaluation of numerical prefactors by allowing comparison of measurable bulk and single-surface properties in terms of these prefactors. This is especially gratifying since, due to its scaling nature, this model is compatible with the known scaling behavior of semidilute bulk polymer solutions: this is generally the relevant concentration regime within adsorbed, interacting polymeric surface phases.

Acknowledgment. We wish to thank Prof. Phil Pincus of the University of California at Santa Barbara for useful comments and suggestions. J.K. thanks Prof. J. F. Joanny and Dr. F. Leermakers for useful cor-

respondence, Tobias Kerle for his help with the data reduction, and the US-Israel Binational Science Foundation, the Israel Science Foundation and the Ministry of Sciences and Arts (Infrastructure grant) for partial support of this work.

References and Notes

(1) Fleer, G.; Cohen-Stuart, M.; Scheutjens, J.; Cosgrove, T.; Vincent, B. *Polymers at Interfaces*; Chapman and Hall; London, 1993.
(2) Scheutjens, J.; Fleer, G. *J. Phys. Chem.* **1979**, *83*, 1619; **1980**, *84*, 178.
(3) de Gennes, P.-G. *Macromolecules* **1981**, *14*, 1637.
(4) de Gennes, P.-G. *Macromolecules* **1982**, *15*, 492.
(5) Klein, J.; Pincus, P. *Macromolecules* **1982**, *15*, 1129.
(6) Ingersent, K.; Klein, J.; Pincus, P. *Macromolecules* **1986**, *19*, 1374; **1990**, *23*, 548.
(7) See for example: de Gennes, P.-G. *Scaling Concepts in Polymer Physics*; Cornell University Press; Ithaca, NY, 1978.
(8) Rossi, G.; Pincus, P. A. *Europhys. Lett.* **1988**, *5*, 641.
(9) Rossi, G.; Pincus, P. A. *Macromolecules* **1989**, *22*, 276.
(10) Semenov, A. N.; Joanny, J.-F. *Europhys. Lett.* **1995**, *29*, 279.
(11) Semenov, A. N.; Bonet Avalos, J.; Johner, A.; Joanny, J.-F. *Macromolecules* **1996**, *29*, 2179.
(12) Johner, A.; Bonet Avalos, J.; van der Linden, C. C.; Semenov, A. N.; Joanny, J.-F. *Macromolecules* **1996**, *29*, 3629.
(13) Klein, J.; Luckham, P. F. *Nature* **1984**, *308*, 836.
(14) Klein, J.; Luckham, P. F. *Macromolecules* **1984**, *17*, 1041.
(15) Luckham, P. F.; Klein, J. *J. Chem. Soc., Faraday Trans.* **1990**, *86*, 1363.
(16) Luckham, P. F.; Klein, J. *Macromolecules* **1985**, *18*, 721.
(17) Klein and Luckham did verify (see ref 14) that for the very dilute solutions used in their experiment, washing does not change the force vs distance profile for the saturated case.
(18) For a recent study of the phase diagram of this system, see: Bekiranov, S.; Bruinsma, R.; Pincus, P. *Phys. Rev. E* **1997**, *55*, 577.
(19) Note, that, in the system of refs 13−15, KNO_3 is present at a concentration of 0.1 M: as a result, the Debye length is on the order of only 1 nm.
(20) Bonet Avalos, J.; Joanny, J.-F.; Johner, A.; Semenov, A. N. *Europhys. Lett.* **1996**, *32*, 97.
(21) Semenov, A. N.; Joanny, J.-F.; Johner, A.; Bonet Avalos, J. *Macromolecules* **1997**, *30*, 1479.
(22) While the repulsive interaction between adsorbed layers in full equilibrium found in refs 20 and 21 represents a qualitative departure from the purely attractive behavior predicted in ref 4, an estimate of the magnitude of the repulsion shows that for colloidal size particles (radius of (0.1−1) μm), the repulsive energy is of the order of (0.1−1)kT. In view of this result, the repulsive effect is not sufficient to account for stabilization in most colloidal systems; it must then be concluded that the standard picture where stabilization effects are associated to irreversible adsorption of polymer chains on the colloidal particles is correct.
(23) Note that, unless the adsorption is extremely weak, inordinately long observation times are required in order to reach experimentally the reversible adsorption regime in a surface force measurement.
(24) Formally, the transition from good solvent (semidilute) to mean field (concentrated) behavior where excluded volume correlations are no longer significant is expected to take place (see: Doi, M.; Edwards, S. F. *The Theory of Polymer Dynamics*; Clarendon Press: Oxford, England, 1986; pp 141−142) when the polymer volume fraction exceeds $\Phi^{**} \approx 1 - 2\chi_F$ where χ_F is the usual Flory polymer solvent interaction parameter. In practice, scaling laws for both local structure and interactions are found to be obeyed for typical systems up to polymer concentrations of several percent (see: Daoud, M.; et al. *Macromolecules* **1975**, *8*, 804; Ferry J. D. *Macromolecules* **1979**, *13*, 1719), a regime which includes most of the concentration range within adsorbed polymer layers.
(25) It can be shown explicitly (see ref 3) that the inclusion of long-ranged van der Waals fields does not perturb the form of the self-similar concentration profile deduced using the short ranged interactions alone.
(26) Edwards, S. F. *Proc. Phys. Soc. London* **1966**, *88*, 255. See also A. K. Dolan and S. F. Edwards, *Proc. Roy. Soc. (London) A* **1975**, *343*, 427 for an early application of the self-consistent mean field method to the problem of interactions between polymer bearing surfaces.
(27) Jones, I. S.; Richmond, P. *J. Chem. Soc., Faraday Trans. 2* **1977**, *73*, 1062.
(28) A number of misprints are present both in ref 4 and in refs 8 and 9. These do not affect the outcome of the calculations but it seems appropriate to list them at this point. In ref 4 the rhs of eq II.1 should contain the monomer volume a^3 (rather than a^{-3}); also, in ref 4 the factor Φ in the denominator of the last term in the integral for the functional, eq III.22, is missing. In refs 8 and 9, the same term (eq 2 of ref 8; eq 25 of ref 9) in the integral should be multiplied by m_0 rather than by m. Finally an overall minus sign is missing in the left-hand side of both eq 5 in ref 8 and eq 28 in ref 9.
(29) Note that both the reduced functions $F(\omega)$ and the reduced surface energy $G(\omega)$ (defined in eq 13) are dimensionless quantities.
(30) Note that $F(\omega)$ coincides with the quantity $\tilde{\Pi}_d(h/D_{sc})$ defined by De Gennes in eq III.51 of ref 4. However, in ref 4 the scale of the $\tilde{\Pi}_d$ axis of Figure 7 is incorrect, so that the actual value of $F(\omega)$ for saturated plates is much smaller than that shown in Figure 7 of ref 4. References 8 and 9 have the correct results for $F(\omega)$.
(31) Tabor, D.; Winterton, R. H. S. *Proc. R. Soc. London, Ser. A* **1969**, *312*, 435.
(32) Israelachvili, J. N.; Tabor, D. *Proc. R. Soc. London, Ser. A* **1972**, *331*, 19.
(33) Derjaguin, B. V. *Kolloid-Z.* **1934**, *69*, 155.
(34) Since $\tilde{\gamma}(h \rightarrow \infty)$ vanishes, $\tilde{\gamma} = \gamma - \gamma_0 - C_i$, where C_i is the limiting value for $h \rightarrow \infty$ of the left-hand side of eq 1 and depends on the coverage (on the ratio Γ/Γ_0). In practice, at small h, $\gamma - \gamma_0$ is much larger than C_i, so that it is appropriate to identify the lhs of eq 18 with the quantity $G(\omega)$ defined in eq 13.
(35) This is simply seen by considering the single-surface self-similar density profile $\Phi(z) \approx \phi_0(a/z)^{4/3}$. For two interacting surfaces the intersurface pressure roughly equals the osmotic pressure at the gap midpoint, so that $\Pi_d \approx \Pi_{osm} = kT/a^3\phi(h)^{9/4} \propto kT/h^3$.
(36) Note that this force−distance curve (1.2 M PEO, Figure 1b, curve c) cannot be used for comparison with the predictions of the model. This is because the part of the curve measured covers only the onset of interactions, and—as for the other M values used—this regime is not described by the scaling model.
(37) Values for the Flory radius R_F of PEO in water are given in Kawaguchi, M.; Masaaki, M.; Takahashi, A. *Macromolecules* **1984**, *17*, 2063.
(38) The actual values of D_{onset} do not scale precisely as $M^{3/5}$ for the different molecular weights, and it is likely that the outer adsorbed segments extend further out than suggested by D_{onset}. The reasons for this have been considered in some detail earlier in ref 39 and have to do with the sensitivity of the SFB in picking up the initial interactions of the outer segments of the opposing adsorbed layers.
(39) Klein, J.; Luckham, P. F. *Macromolecules* **1986**, *19*, 2007.
(40) While this expression for the osmotic pressure was derived originally for an athermal solvent, it has been shown that in a number of cases it applies well, using the appropriate values of α, also for moderate to good solvents in the semidilute regime (see: Ferry, J. D., *loc cit* in ref 24).
(41) (a) Cosgrove, T.; Vincent, B.; Crowley, T. L.; Cohen-Stuart, M. A. In *Polymer Adsorption and Dispersion Stability*, Goddard, E. D., Vincent, B., Eds.; ACS Symposium Series 240; American Chemical Society, Washington, DC, 1984; pp 147−160. (b) Cosgrove, T.; Crowley, T. L.; Ryan, K.; Webster, J. R. P. *Colloids Surf.* **1990**, *51*, 255.
(42) Lee, E. M.; Thomas, R. K.; Rennie, A. R. *Europhysics Lett.* **1990**, *13*, 135.
(43) These values of the volume fraction at the wall are somewhat higher than the expected range of concentrations for semidilute solutions, though we note that, in other polymer/good solvent systems, scaling behaviour has been observed to persist up to comparable concentrations (see: Daoud, M.; et al., *loc cit* in ref 24).
(44) An internal consistency check on these values is provided by eq 5, $a^3\Gamma_0 = 4D_{sc}\Phi_{s0}$, where $a^3\Gamma_0$ equals Γ as defined above in units of length. Over the range of experimental values of D_{sc} and Φ_{s0}, the rhs of this equation, $4D_{sc}\Phi_{s0}$, is in the range 3−4.8 nm, fully consistent with the lhs, $a^3\Gamma_0 \cong \Gamma = 4 \pm 1.5$ nm. We should however note that the adsorbance values for PEO on latex particles in water estimated in the study of ref 41 are lower than for PEO on mica.
(45) Klein, J. *J. Chem. Soc., Faraday Trans. 1* **1983**, *79*, 99.

MA9709314